applied sciences

MDPI

Article

Assessing the Compaction Quality of Dolomitic Asphalt Pavements Using Ground Penetrating Radar

Enas Abdelsamei, Diaa Sheishah, Zalán Tobak, Ahmed M. Ali, Károly Barta, Abdelouahed Fannakh, Gergő Magyar, Viktória Blanka-Végi and György Sipos *

Department of Geoinformatics, Physical and Environmental Geography, University of Szeged, Egyetem u. 2-6., 6722 Szeged, Hungary; enas.mohammed@nriag.sci.eg (E.A.); geo_diaa@nriag.sci.eg (D.S.); tobak@geo.u-szeged.hu (Z.T.); ahmed.mahmoud@nriag.sci.eg (A.M.A.); barta@geo.u-szeged.hu (K.B.); abdelouahed.fannakh@gmail.com (A.F.); magyar.gergo94@gmail.com (G.M.); blankav@geo.u-szeged.hu (V.B.-V.)
* Correspondence: gysipos@geo.u-szeged.hu

Abstract: The quality of newly constructed pavement depends mostly on compaction, which is essential for ensuring the pavement's longevity and performance. Traditional methods of evaluating pavement compaction and density, such as core sampling and nuclear gauge measurements, are often time-consuming and invasive and provide only a limited amount of data at a low spatial resolution on the potential air void content of the asphalt layers. The present study aimed to assess the specific gravity (G_{mb}) of a dolomitic asphalt mixture at different degrees of compaction using GPR techniques. Relative density (RD) maps were generated to visualize the spatial homogeneity of the asphalt density. Nuclear density gauging was applied for the calibration, and cores were used to validate the results. The survey was conducted on two recently paved roads in Szeged, Hungary. After testing various approaches, it was found that applying horn antennas and the surface reflection (SR) method is the most feasible way to obtain reliable and accurate dielectric permittivity (ε) data. Based on the measurements, clear relationships were found between dielectric constants, G_{mb}, and aggregate size. The findings highlight that it is possible to indirectly determine the G_{mb} of asphalts composed of dolomite and limestone aggregates using GPR, with aggregate sizes ranging from 11 mm to 25 mm and G_{mb} values between 2.43 and 2.57 g/cm^3. Consequently, a robust function was developed, which can be applied to other asphalts with similar compositions.

Keywords: Ground Penetrating Radar (GPR); dielectric permittivity; specific gravity; relative density; aggregate size

Academic Editors: Deshan Feng, Xun Wang and Bin Zhang

Received: 4 January 2025
Revised: 20 February 2025
Accepted: 24 February 2025
Published: 26 February 2025

Citation: Abdelsamei, E.; Sheishah, D.; Tobak, Z.; Ali, A.M.; Barta, K.; Fannakh, A.; Magyar, G.; Blanka-Végi, V.; Sipos, G. Assessing the Compaction Quality of Dolomitic Asphalt Pavements Using Ground Penetrating Radar. *Appl. Sci.* **2025**, *15*, 2501. https://doi.org/10.3390/app15052501

1. Introduction

The dielectric properties of pavement materials are crucial in GPR investigations [1]. The dielectric permittivity (ε) of a substance refers to its ability to store the applied electric field, with the dielectric constant (ε_r) representing the ratio of its permittivity to that of the vacuum (ε_0) [2]. Previous studies, such as those by Loizos and Plati [3,4], proposed three calibration methods: core calibration, laboratory ε determination, and reflection amplitude calibration, all suitable for pavement evaluation. This paper distinguishes itself by using horn antennas and the surface reflection method to indirectly determine the specific gravity (G_{mb}) of dolomitic asphalt mixtures, developing a general function applicable to similar asphalt compositions and offering a more streamlined and widely applicable approach than the methods discussed.

The ε of asphalt pavement can be measured using the time-of-flight (TOF) and the surface reflection (SR) methods. The TOF method determines permittivity by analyzing the electromagnetic (EM) wave travel time, or TOF, within the asphalt layer, using in situ core samples to derive the dielectric constant based on the known layer thickness and GPR signal properties. The SR method estimates permittivity by measuring the SR amplitude from the GPR signal and comparing it with a calibration signal amplitude obtained from the EM reflection off a metal plate on the pavement's surface [5].

The main reason for variations in asphalt dielectric constants is related to the composition of the material and its physical properties [6–8], such as its aggregate type, bulk density, bitumen content, and air void content [9–12]. Among these constituents, the aggregate type has the greatest versatility concerning the ε [13]. A wide range of rock types are used as aggregates, though certain types are preferred due to their resistance to fragmentation and polishing. Two widely used rock types are dolomite and limestone [14], with a density similar to that of volcanic and crystalline rocks but with a notably different ε [15,16].

Besides aggregate properties, the density of the asphalt mixture is also a key factor in the performance of flexible pavements. The air void content should range between 3% and 8% [17]. A high air void content leads to moisture damage, binder oxidation, pavement raveling, and cracking. Conversely, a low air void content increases stiffness and reduces the rutting potential and possible bleeding [18]. In dense-graded asphalt mixtures, if the air void content falls below 3%, it can lead to significant permanent deformation and shoving [17,18]. Asphalt pavements' G_{mb} and air void ratios are inversely related: as the air void ratio increases, the G_{mb} of asphalt decreases. Thus, the air void ratio is also used to assess the asphalt density. Both parameters are largely influenced by the degree of asphalt compaction. Compaction of the asphalt layer minimizes the presence of low-ε air in the asphalt mixture, while the volumetric ratios of high-dielectric asphalt and rock are augmented. Consequently, this process leads to elevated ε values [19,20].

Compaction is critical for achieving the desired density of the asphalt layers; in other words, the quality of the newly constructed pavement depends mostly on the quality of the compaction. In the process of asphalt pavement construction, the paver initially places the asphalt mixture on a bound or unbound base. Subsequently, compactors traverse the loose asphalt mat, eliminating air voids from the mixture. With each pass of the compactor, the air void content decreases. Previous work has demonstrated that inadequate asphalt compaction can result in excessive rutting, cracking, raveling, potholing, and water seepage [21].

Therefore, determining the G_{mb} or air void content of asphalt layers, i.e., assessing the compaction's properness, is important when evaluating the pavement quality and durability. The two commonly employed approaches for the evaluation of compaction quality are (1) laboratory assessment of cores and (2) field density gauging, including nuclear and non-nuclear density measurements. Previous studies have suggested that Ground Penetrating Radar (GPR) can also be utilized as a non-nuclear method to assess the compaction quality and monitor the compaction process during asphalt pavement construction [22,23]. However, in many countries, in situ nuclear gauge measurements are still used in standard applications [24–27]. The disadvantage of this latter method is that it gives low spatial resolution and at-a-point information on G_{mb}, and the operation of the device requires special knowledge and permissions.

The first aim of the present research was to apply different GPR techniques in the assessment of dielectric constants and to determine the most reliable and convenient way of conducting in situ measurements using validation data obtained from nuclear gauge and laboratory pavement core tests. The extensive measurements during the repeated compaction of the investigated pavement also allowed the establishment of a function

between dielectric constants and G_{mb}. Consequently, by also involving literature data, we attempted to establish a more general model for the GPR assessment of G_{mb} and relative density (RD) on dolomitic pavements.

2. Description of Test Sections

The studied sections are located in Szeged, Hungary. Two newly constructed two-lane residential roads, Section I. and Section II., were chosen to conduct the survey (Figure 1). The lengths of Section I. and Section II. are 220 m and 240 m, respectively, while the width of both sections is 6 m.

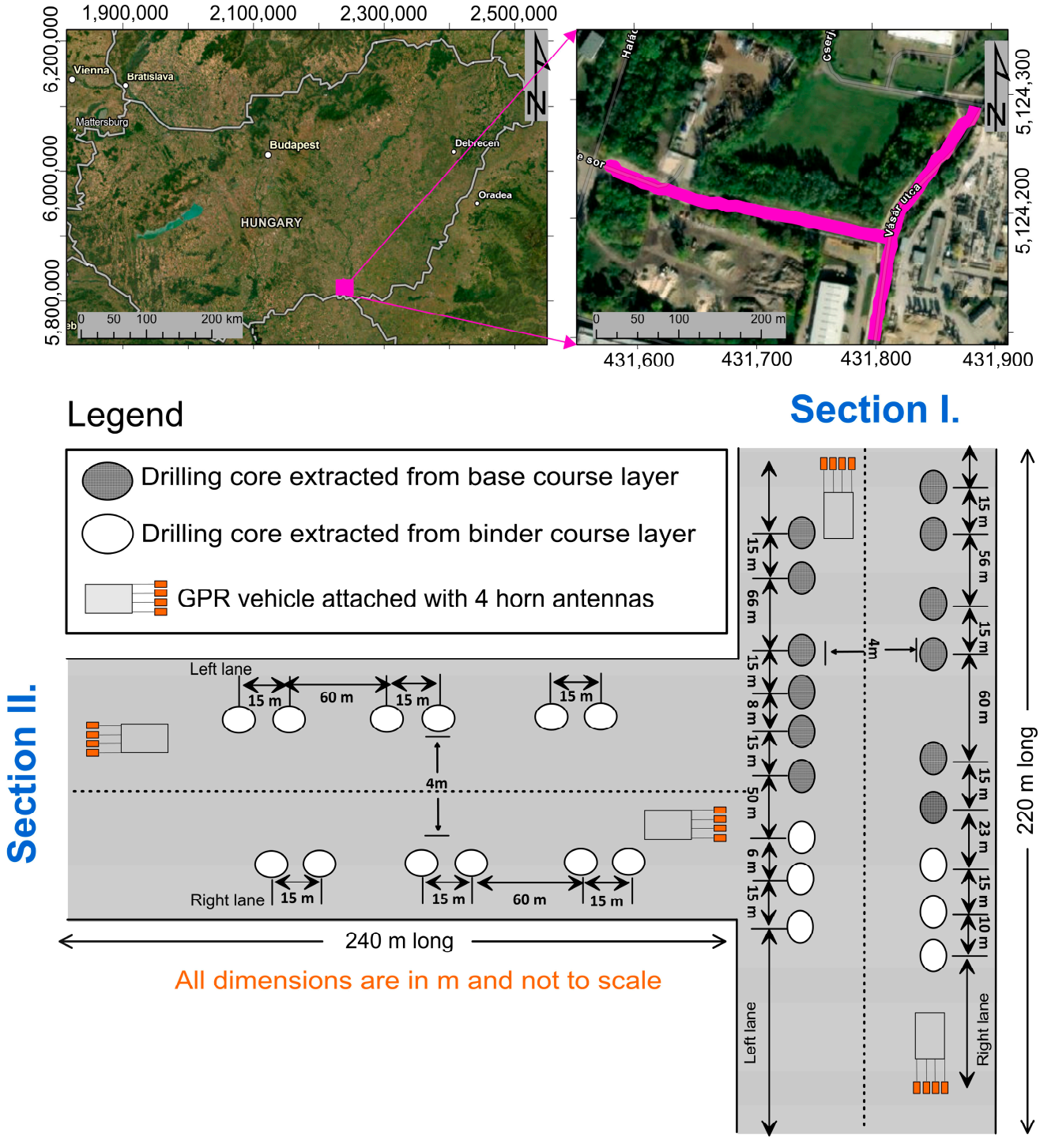

Figure 1. The location of the studied residential road sections.

The pavement structure of the analyzed roads was as follows (Figure 2):

1. 4.0 cm AC 11 wearing course.
2. 7.0 cm AC 22 binder course.
3. 8.0 cm AC 22 base course.
4. 20.0 cm FZKA 0/63 unbound granular base (refines upward from 0/63 to 0/32 until 0/22 mm).
5. 20.0 cm sandy gravel protection layer.

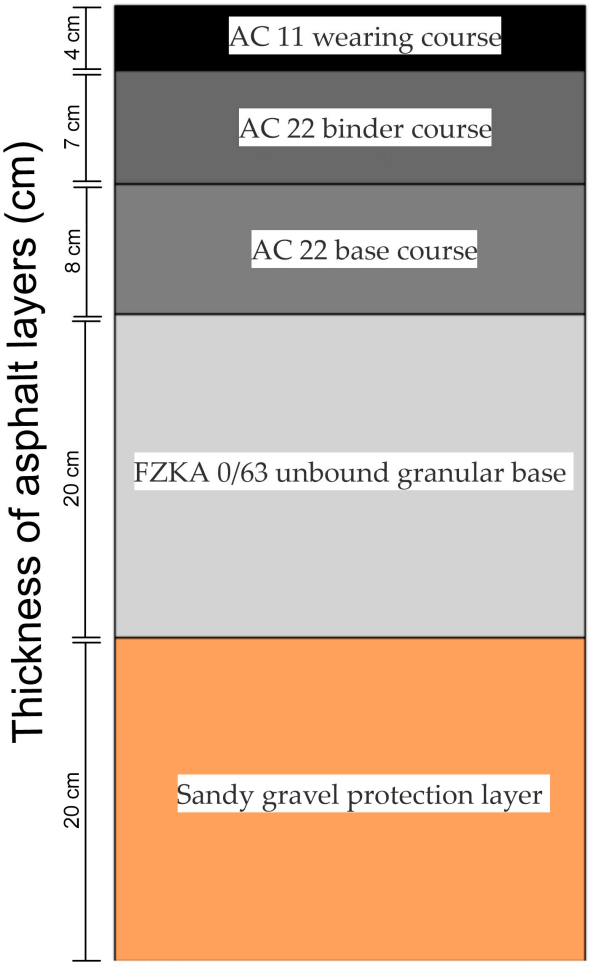

Figure 2. A cross-section of the pavement structure, with the wearing course, binder course, base course, unbound granular base, and sandy gravel protection layer.

In both asphalt mixes (AC 11 and AC 22), the aggregate rock type was dolomitic limestone, and the proportion of bitumen was 4.1% by weight. The unbound granular base was also composed of dolomitic limestone [12].

AC 11 and AC 22 are common asphalt mixes (AC) used in road construction, with the numbers indicating the grading of the aggregates; AC 11 has smaller aggregates than AC 22. AC 11 is typically used for wearing courses, while AC 22 is used for binder and base courses. These mixes are standard in Europe for creating durable, high-performance pavements.

3. Data and Methods

3.1. GPR Data Acquisition

GPR surveys were carried out by using two 1 GHz and two 2 GHz air-coupled GPR antennas with a SIR-30 control unit from Geophysical Survey Systems, Inc., Nashua, NH, USA [28] to determine the relative permittivity (Figure 3). The horn antennas were

suspended at the rear of a vehicle at 0.5 m from the pavement surface (Figure 4). The positioning was made using a GPS antenna mounted on the vehicle's roof. Furthermore, a high-resolution Distance Measuring Instrument (DMI) sensor was attached to the rear wheel to ensure the precise triggering of the GPR scans at predetermined intervals. The survey car was driven at a speed of 15 km/h during the survey. At the beginning of the survey, the inline and crossline offsets were manually determined to adjust the GPS location. The GPR signals were collected at a frequency of 50 scans per meter, with a scan rate of 340 scans per second. The units per mark were set to 5, and the samples per scan were configured to 2048. A one-point gain (flat gain) was used throughout the surveys. The measurement time, or time window, was set to 30 ns for the 1 GHz antenna and 25 ns for the 2 GHz antenna. Full-coverage horn antenna GPR measurements were performed after constructing the sub-base layer, the base course, the binder course, and the wearing course; thus, the measurements were repeated four times.

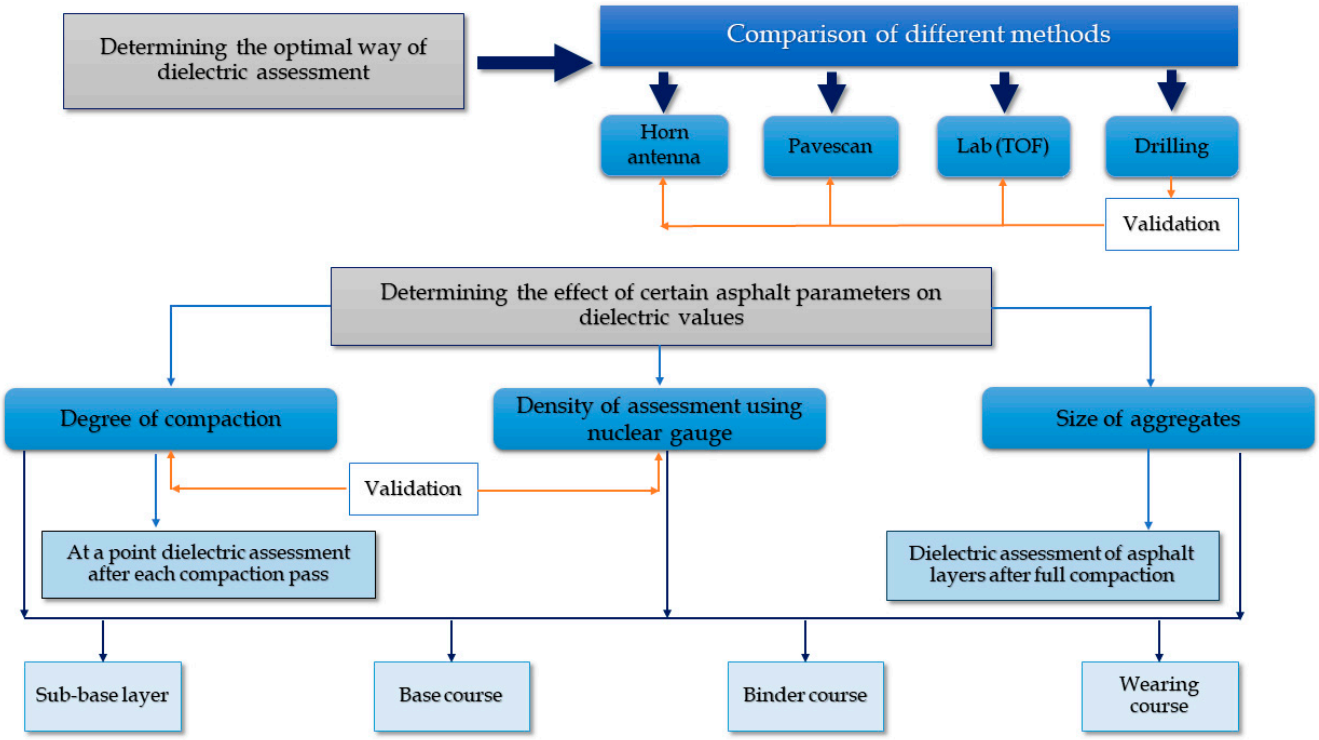

Figure 3. A flowchart showing the course of the analysis.

3.2. PaveScan Data Acquisition

Besides horn antennas, a PaveScan RDM 1.0 device from Geophysical Survey Systems, Inc. [28], mounted with three sensors, was also used to determine the relative permittivity (Figure 3). The distance between the sensors was set to 1.2 m to cover the width of the lanes effectively. Before the data collection, the sensors were lifted 0.6 m off the ground to perform air calibration. Next, the metal plate calibration was performed by centering the plate 2.5 cm below the sensor. The distance mode was used during the survey, and the data collection speed was 5 km/h. The PaveScan measurements, covering the entire length of the road sections, were performed once after the construction of each layer.

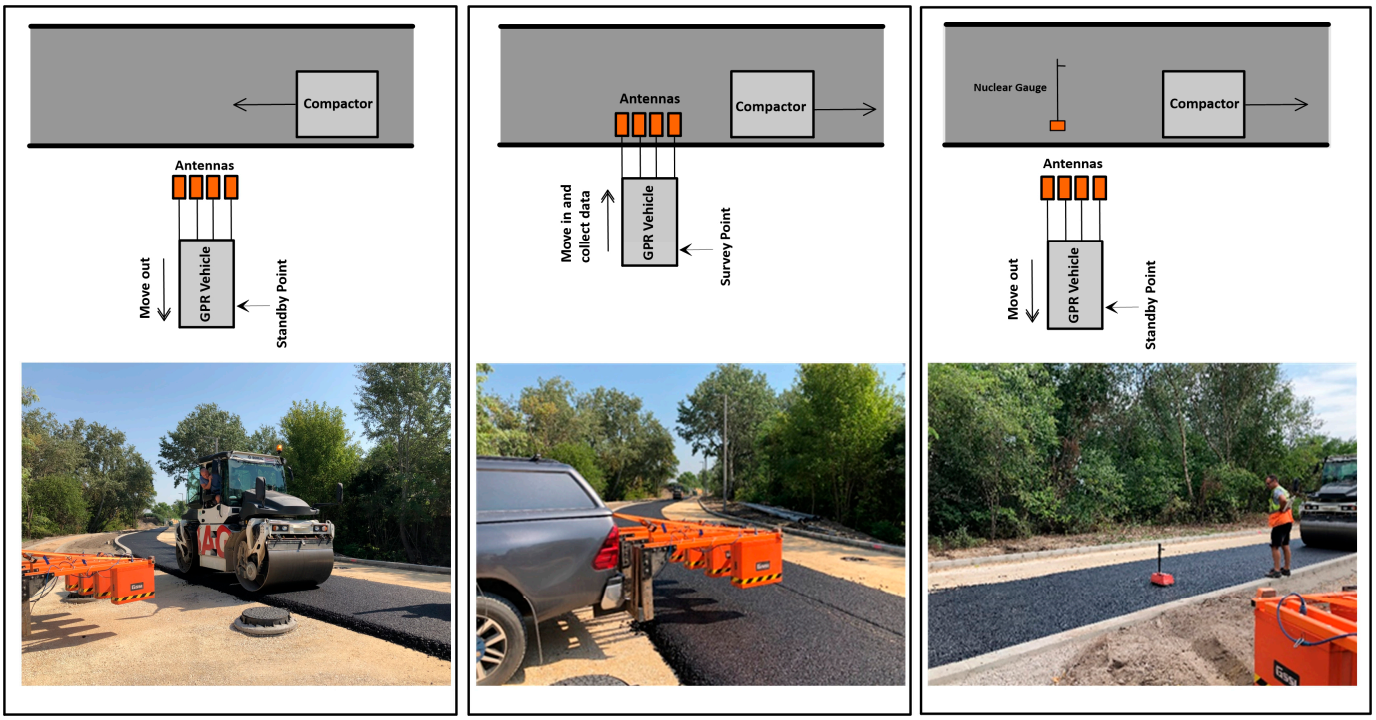

Figure 4. The procedure of repeated stationary GPR and nuclear gauge measurements. From left to right: vibratory roller pass, GPR horn antenna measurements, nuclear gauge measurements.

3.3. Calibration and Core Sampling

Simultaneously with the GPR data acquisition, cores were also extracted for calibration (Figure 1). In all, 18 cores were extracted from Section I. Twelve cores were extracted after laying the base course layer, and six cores were extracted after laying the binder course. In terms of Section II., twelve cores were extracted after laying the binder course, as shown in Figure 1. GPS recorded the position of the cores. The cores were subjected to laboratory measurements using a SIR 3000 GPR system with a 1 GHz ground-coupled antenna. For the measurements, the cores were placed in a plastic box with a metal plate on the bottom, leading to a complete base reflection. The plastic box was then filled with crushed andesite to lessen wave diffraction and ensure that the ground-coupled 1 GHz antenna was placed on a flat surface. The ε was calculated using the TOF method.

3.4. Compaction and ε Relationship Measurement

To explore the relationship between the degree of compaction and the change in the dielectric constant, stationary GPR data were collected at the same location at the construction site after each pass of a vibratory roller during the laying of each asphalt layer (Figure 4). For the two test sites, seven short GPR profiles were measured after each roller pass and after laying each asphalt layer. The measurements were carried out in time mode. Immediately after the compactor completed one pass, the GPR vehicle moved toward the lane to place the antenna above the pavement. The data collection was made in time mode for approximately 10 s. The GPR vehicle moved back to its original position, as shown in Figure 4. Following the GPR measurement, a density reading was taken by a CPN MC-3 PORTAPROBE-type nuclear gauge [29]. The backscatter mode was chosen for the measurements [30]. The device was placed on the compacted layer after warming up and determining the GPS position of the measurement point.

4. Data Processing

The collected GPR data were processed using GSSI's RADAN 7 software [28]. The raw data were processed to remove noise and to improve the signals. First, metal plate calibration was performed on the data files, and then inline and crossline values were edited manually to prepare the GPR data files for further analysis and to determine the true track of the measurements, respectively. Next, the program automatically performed reflection picking after manually selecting the reflection picking function to reduce undesired signal noise and improve reflections from the pavement layers. The processing was continued by filtering the data, including (1) a triangular finite impulse response (FIR) filter, applying a weighted moving average procedure emphasizing the filter's center rather than the ends of it; (2) a horizontal filter (stacking), merging neighboring radar scans and delivering a single scan through a simple running average; and (3) vertical filters, i.e., a low pass filter to remove high-frequency noise (2 GHz and 4 GHz thresholds for the 1 GHz and 2 GHz antennas, respectively) and a high pass filter to remove low-frequency noise (250 MHz and 500 MHz thresholds for the 1 GHz and 2 GHz antennas, respectively). Finally, the gain properties were set by applying an exponential gain function. The gain was set at 5–7 points. A horizontal background removal filter was applied in certain profiles, particularly those measured along both sections where the data exhibited significant interference or noise from unwanted reflectors—potentially obscuring critical measurements. However, this filter was not required for the GPR profiles collected after each roller pass and following the placement of each asphalt layer. In this case, the filter's length must always exceed the length of the data's longest horizontal "real" reflector [28].

5. Assessment of Physical Properties Using GPR Data

Maser [24] discussed the principles of using GPR reflections to compute layer properties in detail. By automatically monitoring the amplitudes and time delays between peaks, it is possible to calculate layer ε values using the SR method. The ε_{r1} is calculated by comparing the reflection amplitudes from an asphalt surface and a metal plate surface (100% reflection), as Equation (1) indicates.

$$\varepsilon_{r1} = \left[\frac{1 + \left(\frac{A_0}{A_p}\right)}{1 - \left(\frac{A_0}{A_p}\right)}\right]^2 \quad (1)$$

where ε_{r1} is the ε of the surface course layer, A_0 is the amplitude of the reflection from the surface course layer, and A_p is the amplitude of the reflection from a metal plate.

The ε of the second asphalt layer can be calculated as the following Equation (2) using the value ε_r computed in Equation (1) [2,31]:

$$\varepsilon_{r2} = \varepsilon_{r1}\left[\frac{1 - \left(\frac{A_{0,1}}{A_p}\right)^2 + \left(\frac{A_{0,2}}{A_p}\right)}{1 - \left(\frac{A_{0,1}}{A_p}\right)^2 - \left(\frac{A_{0,2}}{A_p}\right)}\right]^2 \quad (2)$$

where ε_{r2} is the ε of the second binder course layer (layer 2). $A_{0,1}$ and $A_{0,2}$ are the amplitudes of the reflection from the second binder course layer (layer 2) and first binder course layer (layer 1), respectively.

Consequently, the ε of any further layers (ε_n) can be calculated using Equation (3).

$$\varepsilon_n = \varepsilon_{n-1}\left[\frac{1 - \left(\frac{A_{0,1}}{A_p}\right)^2 + \sum_{i=1}^{n-2}\gamma_i\frac{A_{0,i+1}}{A_p} + \frac{A_{0n}}{A_p}}{1 - \left(\frac{A_0}{A_p}\right)^2 + \sum_{i=1}^{n-2}\gamma_i\frac{A_{0,i+1}}{A_p} - \frac{A_{0n}}{A_p}}\right]^2 \quad (3)$$

where γ_i is the reflection coefficient at the interface between the two following layers, and n stands for the specific layer and can be calculated using Equation (4) [2].

$$y_i = \frac{\sqrt{\varepsilon_{r,i}} - \sqrt{\varepsilon_{r,i} + 1}}{\sqrt{\varepsilon_{r,i}} + \sqrt{\varepsilon_{r,i} + 1}} \quad (4)$$

where $\varepsilon_{r,i}$ is ε of the i^{th} layer. A function was established for the G_{mb} and ε of each asphalt layer using density gauge measurements during the asphalt compaction and simultaneous GPR measurements. This function was applied to map the asphalt G_{mb} on the investigated road section spatially. The quality assessment of road structures is primarily based on the percent of the air void (AV) of the asphalt layers, and this parameter was estimated using Equation (5).

$$AV = G_{mm} - G_{mb}/G_{mm} \quad (5)$$

Laboratory measurements were made on samples from the AC 11 (wearing course) and the AC 22 (binder and base courses) asphalt mixtures [12]. The measured theoretical maximum G_{mb} of the samples was as follows: G_{mm} AC 11 = 2436 kg/m^3, G_{mm} AC 22 = 2572 kg/m^3.

G_{mm} is the theoretical maximum specific gravity measured in the laboratory of the HMA, and G_{mb} is the specific gravity, which is estimated in the field using GPR measurements.

Finally, the in situ RD of the analyzed layers was calculated using the following formula:

$$RD = 1 - AV = G_{mb}/G_{mm} \quad (6)$$

The obtained values for the above parameters were spatially interpolated using kriging and visualized with Surfer v.16.

6. Results

6.1. Comparability and Accuracy of ε Measurements

We conducted a comparative study using field and laboratory validation to determine the most efficient measurement approach—specifically, the horn antenna or PaveScan—for further analysis of pavement characteristics. By comparing the results (Table 1), we found that the average ε values of the base course, binder course, and wearing course, calculated by the horn antenna and PaveScan for Sections I. and II, yielded similar results.

Table 1. Comparison of average ε values for different pavement layers using horn antenna and PaveScan in Sections I. and II.

	Section I.		Section II.	
Layer	**Horn Antenna**	**PaveScan**	**Horn Antenna**	**PaveScan**
Base Course	5.87	5.86	5.65	5.67
Binder Course	6.1	6.09	5.63	5.76
Wearing Course	4.42	4.73	4.52	4.23

When validating the above results of the base course and binder course layers using cores (the wearing course was not cored), it was found that for Section I., the relative deviation of the PaveScan dielectric values from the core-derived laboratory data was considerably higher than the relative deviation experienced in the case of the GPR horn antenna measurements, as shown in Table 2, for Section II. It was found that the relative deviation of the PaveScan dielectric values from the core-derived data was also considerably higher than the relative deviation experienced based on the horn antenna measurements,

as shown in Table 2. It was also noticed that the dielectric constants of the surface course had the lowest values, which were surveyed by either the horn antenna or the PaveScan device, probably because the smallest grain size characterized this layer compared to the other layers.

Table 2. Comparison of relative deviation (%) between PaveScan and horn antenna dielectric values and core-derived laboratory data for base and binder course layers in Sections I. and II.

		Section I.			Section II.		
Layer	**Measurement Method**	**Min Deviation (%)**	**Max Deviation (%)**	**Mean Deviation (%)**	**Min Deviation (%)**	**Max Deviation (%)**	**Mean Deviation (%)**
Base Course	PaveScan	1.03	6.36	4.46	0.14	2.81	1.58
Binder Course		0.42	4.94	2.45	0.39	7.88	3.84
Base Course	Horn Antenna	0.31	2.41	1.4	0.22	1.94	1.05
Binder Course		0.39	3.16	1.88	0.2	7.72	3.34

In general, the horn antenna values were closer to the core data. In other words, horn antenna measurements can estimate dielectric constants very well, and their accuracy is higher than PaveScan measurements. However, in the case of both devices, the assessment of ε was made using the SR method, while the laboratory assessment was made using the TOF method. Nevertheless, the results underline the flexible use of horn antenna systems in determining the ε of pavement layers (Figure 5).

To assess the accuracy of the horn antenna and PaveScan instruments applied in the field, a detailed comparison was made between the laboratory test measurements, performed for each layer separately, and the field data obtained by the horn antenna and PaveScan measurements after the compaction of each layer (Figure 6). All of the core samples were applied to investigate comparability. Laboratory measurements were formulated to provide an independent ε value for the comparisons. Initially, we established a relationship between the on-site ε values obtained by the horn antenna measurements just before the coring was made using the SR method and the ε values obtained in the laboratory from the cores themselves by the ground-coupled antenna using the TOF method (Figure 6a). The results showed a direct proportional relationship with a high coefficient of determination (R^2 = 0.83), indicating a strong correlation between the ε values obtained with the two approaches. Subsequently, we plotted the at-a-point results of the PaveScan measurements using the SR method against the laboratory data (Figure 6b). A very similar coefficient of determination was obtained in this case (R^2 = 0.82). However, the regression line in terms of the horn antenna results approximates the line of equality much better than the regression obtained using the PaveScan measurements; thus, the ε obtained by using the horn antenna exhibits closer agreement with the laboratory measurements. Based on these findings, we can confidently conclude that the SR horn antenna values can be effectively utilized for the reliable investigation of ε, and the data obtained are reliable for further analyses in this study.

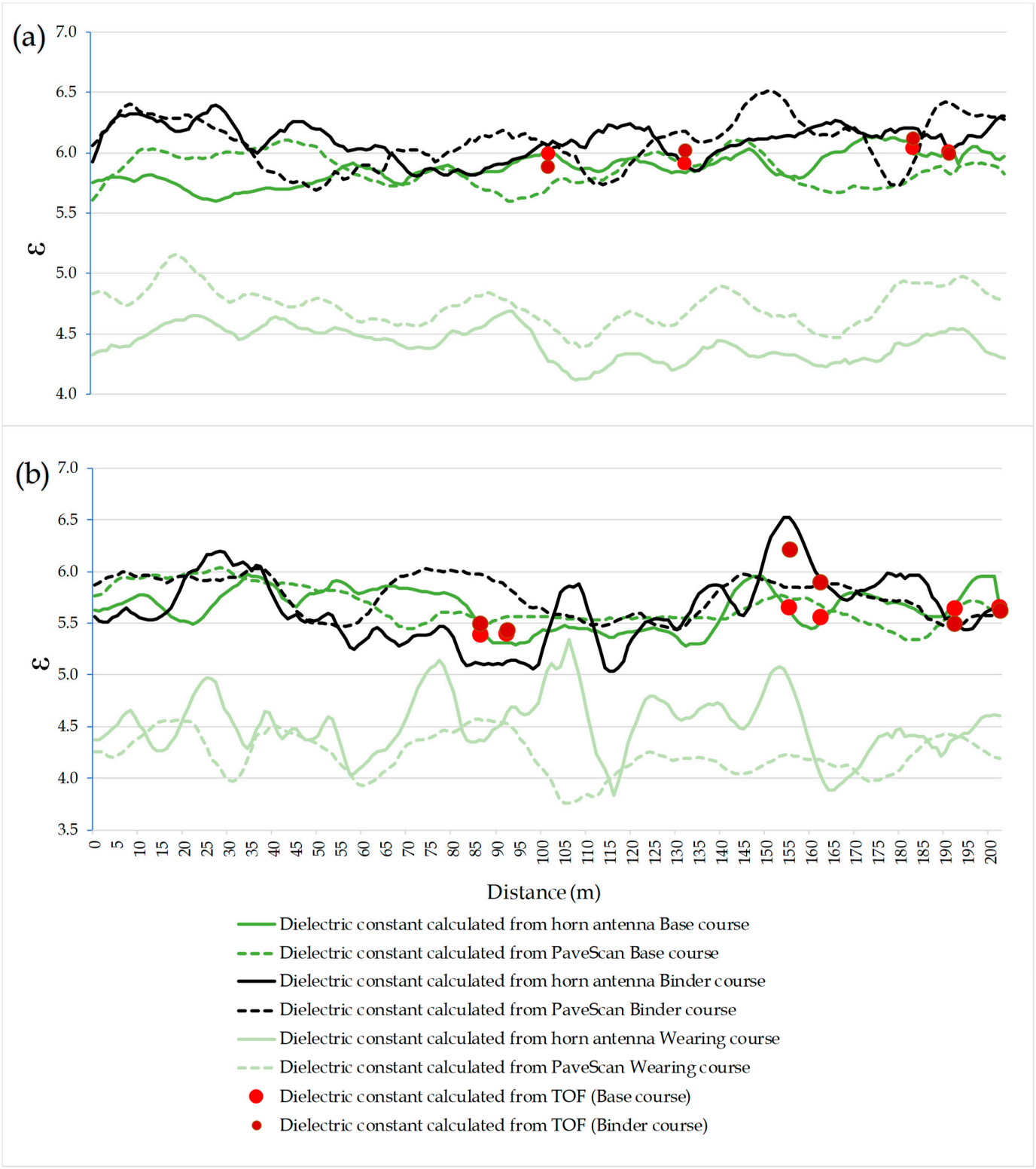

Figure 5. Longitudinal profile of ε values measured by horn antenna method and PaveScan device; (**a**) Section I., (**b**) Section II. Red and maroon dots represent core-derived ε values at coring locations.

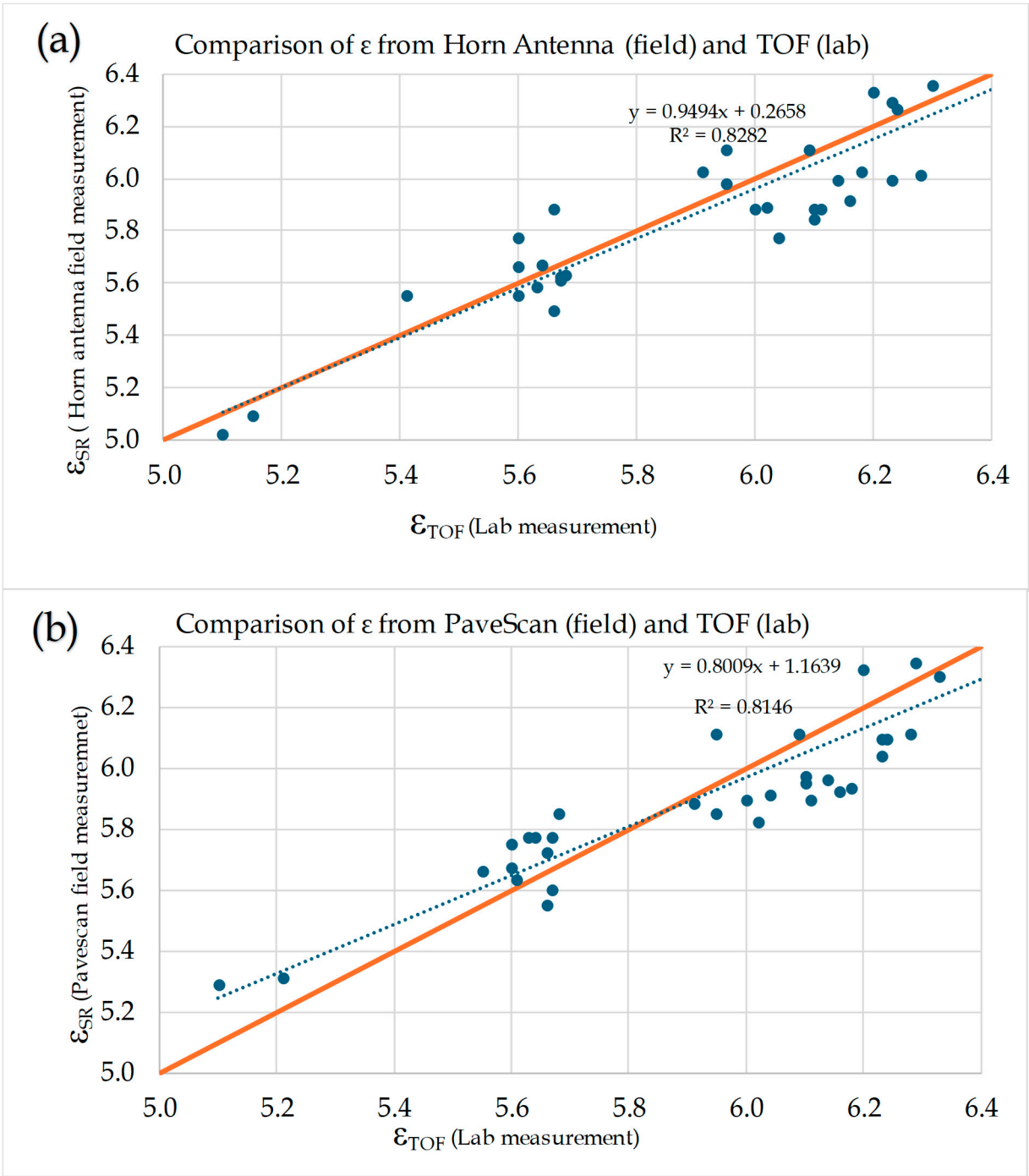

Figure 6. A comparison of ε from the (**a**) SR horn antenna (field measurement) and TOF (laboratory measurement) methods; (**b**) SR PaveScan (field measurement) and TOF (laboratory measurement) methods using the core samples. The orange line represents the line of equality.

6.2. Effect of G_{mb}, Aggregate Size, and Compaction on ε

By understanding how the G_{mb} and aggregate size affect dielectric values, a valuable tool can be developed to assess the compaction quality, the material homogeneity, and the prediction of the structural performance of the pavement. Nuclear gauge G_{mb} data was plotted against the GPR results on ε to establish relationships among the above parameters (Figure 7). The G_{mb} was measured on each layer after each compaction pass. In the case of each layer, a clear, direct relationship was found between density and ε, and the coefficient of determination was, in most cases, higher than 0.9. The layers

appeared at different parts of the graph, and the slope of the linear functions between the plotted parameters was also different for each. This occurs because the variation in slope indicates that different asphalt layers have unique dielectric–density relationships, which are influenced by material properties such as aggregate size (d_{max}), compaction level, and asphalt content. Understanding these distinctions is important for accurately interpreting the GPR results. The highest G_{mb} and ε values were found in terms of the sub-base course (ρ: 2.60–2.80 g/cm^3 and ε: 8.77–10.88); the binder and base course exhibited medium values ((ρ: 2.30–2.54 g/cm^3 and ε: 5.13–6.46)) on average; and the wearing course had the lowest values (ρ: 2.11–2.29 g/cm^3 and ε: 3.77–4.70). The results show a clear relationship between the aggregate size (d_{max}) and the dielectric values.

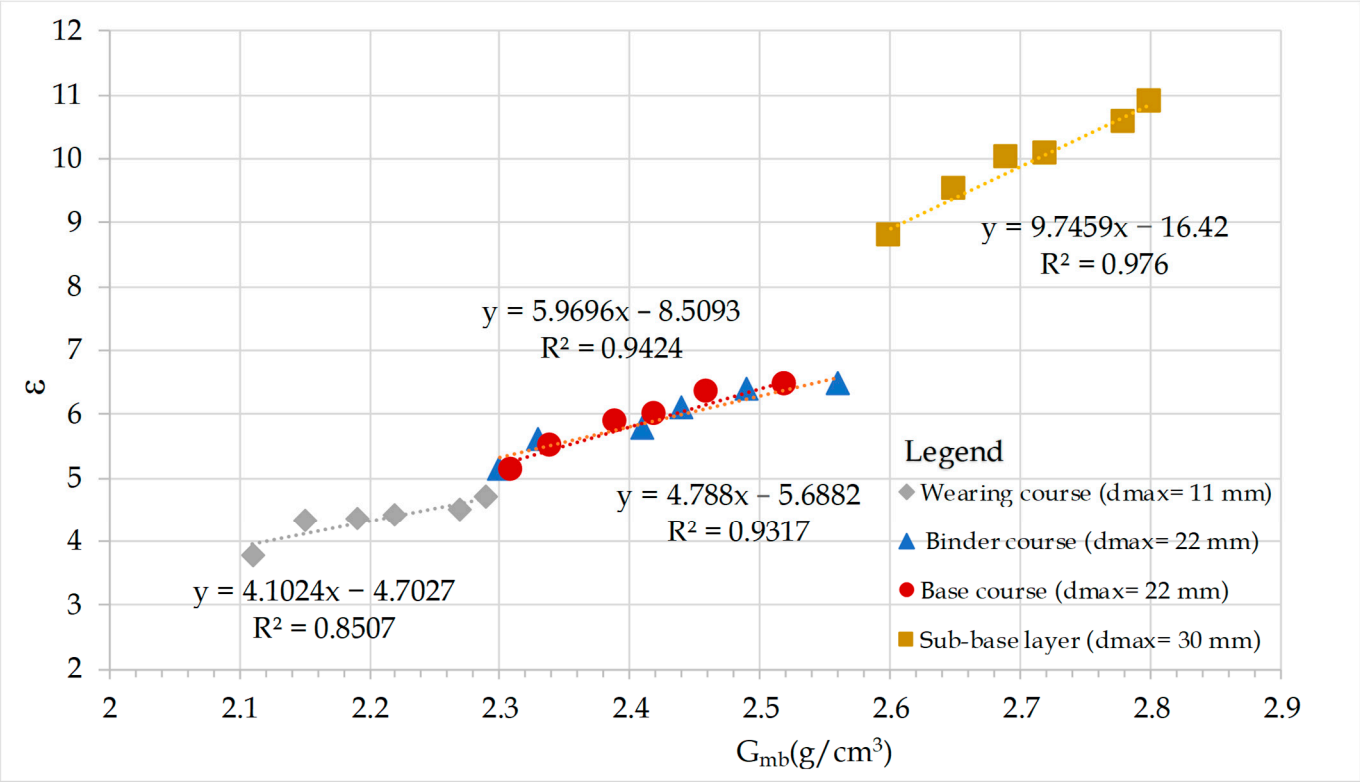

Figure 7. The relationship between the G_{mb}, measured by the nuclear gauge, and the ε, measured by the horn antenna, during the compaction process of each layer (1, 2, 3, 4, 5, 6, and 7 correspond to the number of compaction passes).

We can read from Figure 7 that larger aggregates generally lead to a higher G_{mb} because they reduce the overall porosity. However, smaller aggregates allow for a more uniform and efficient compaction process, which enhances density but may also retain a higher concentration of air voids if not adequately compacted. The compaction process was efficient in the case of the wearing course, which contained smaller aggregates. However, it did not fully eliminate the air voids, leading to a slightly lower G_{mb} than the coarser layers. In contrast, the binder course and base course layers, characterized by a moderate aggregate size, contained moderate air voids. Consequently, the binder course and base course showed better compaction, leading to higher density than the wearing course. The high dielectric values of the sub-base course are primarily due to its larger aggregate size, which influences the air void distribution and compaction efficiency. While dolomitic aggregates may have a naturally higher dielectric constant, the dominant factor in this context is the aggregate size, as it directly affects the layer's density and air void content. Six compaction passes reached the maximum density and dielectric values (Table 3). We

found that the ε for all layers reached a relatively stable value, indicating the achievement of maximum mixture densities. These compaction curves can serve as a valuable reference for determining the optimal number of compaction passes required to achieve the maximum mixture density. Additionally, the point at which the dielectric and density values show negligible changes—observed after six compaction passes—could provide a reference for future research studies. Overall, the assessment revealed the relationship between the ε and G_{mb}, providing insights into the compaction and characteristics of the different asphalt layers.

Table 3. The G_{mb} and ε values during the compaction process for each pavement layer.

Number of Compaction Passes	Sub-Base Course		Base Course		Binder Course		Wearing Course	
	G_{mb}	ε	G_{mb}	ε	G_{mb}	ε	G_{mb}	ε
1	2.6	8.77	2.31	5.11	2.3	5.11	2.11	3.77
2	2.65	9.5	2.34	5.49	2.33	5.49	2.15	4.31
3	2.69	9.99	2.39	5.88	2.41	5.88	2.19	4.36
4	2.72	10.05	2.42	5.99	2.44	5.99	2.22	4.41
5	2.78	10.55	2.46	6.33	2.49	6.33	2.27	4.50
6	2.8	10.88	2.52	6.44	2.56	6.44	2.29	4.70
7	2.8	10.88	2.52	6.44	2.56	6.44	2.29	4.70

6.3. The RD of Asphalt Layers

Standardized at-a-point nuclear gauge measurements provide only a limited number of data and a low spatial resolution of the potential air void content of asphalt layers. Based on the systematic tests made during the compaction process and the equations determined, detailed maps were generated on the RD of the different asphalt layers to visualize the parameter's spatial homogeneity. RD maps can be important in predicting the pavement's long-term performance, supporting maintenance strategies, and facilitating the detection of different defects.

In general, we found that the RD values showed significant differences across the pavement's depth and along the roadway section. Across the depth of the pavement, the lowest RD values were experienced regarding the wearing course (Table 3 and Figure 8). Based on the relationships in Figure 7, this result occurred because the AC 11 mixture can incorporate more air voids, which simultaneously decreases its density and ε compared to the applied AC 22 mixture.

In the case of both sections, the RD of the base course was higher than the RD of the binding course, even though both layers were constructed from the same mixture, and the same number of roller passes were applied during their construction. This suggests that the compaction of the binding and wearing courses led to the additional compaction of the base course, even though the base course had cooled down by the time of the construction of the overlying layers. Consequently, the RD of the base course was found to be the highest of the investigated layers. However, the base course had the highest variability, or standard deviation (SD) of RD values (Table 3 and Figure 8), referring to a less uniform compaction, probably due to the uneven sub-base layer. The most uniform compaction was achieved in the case of the binding course.

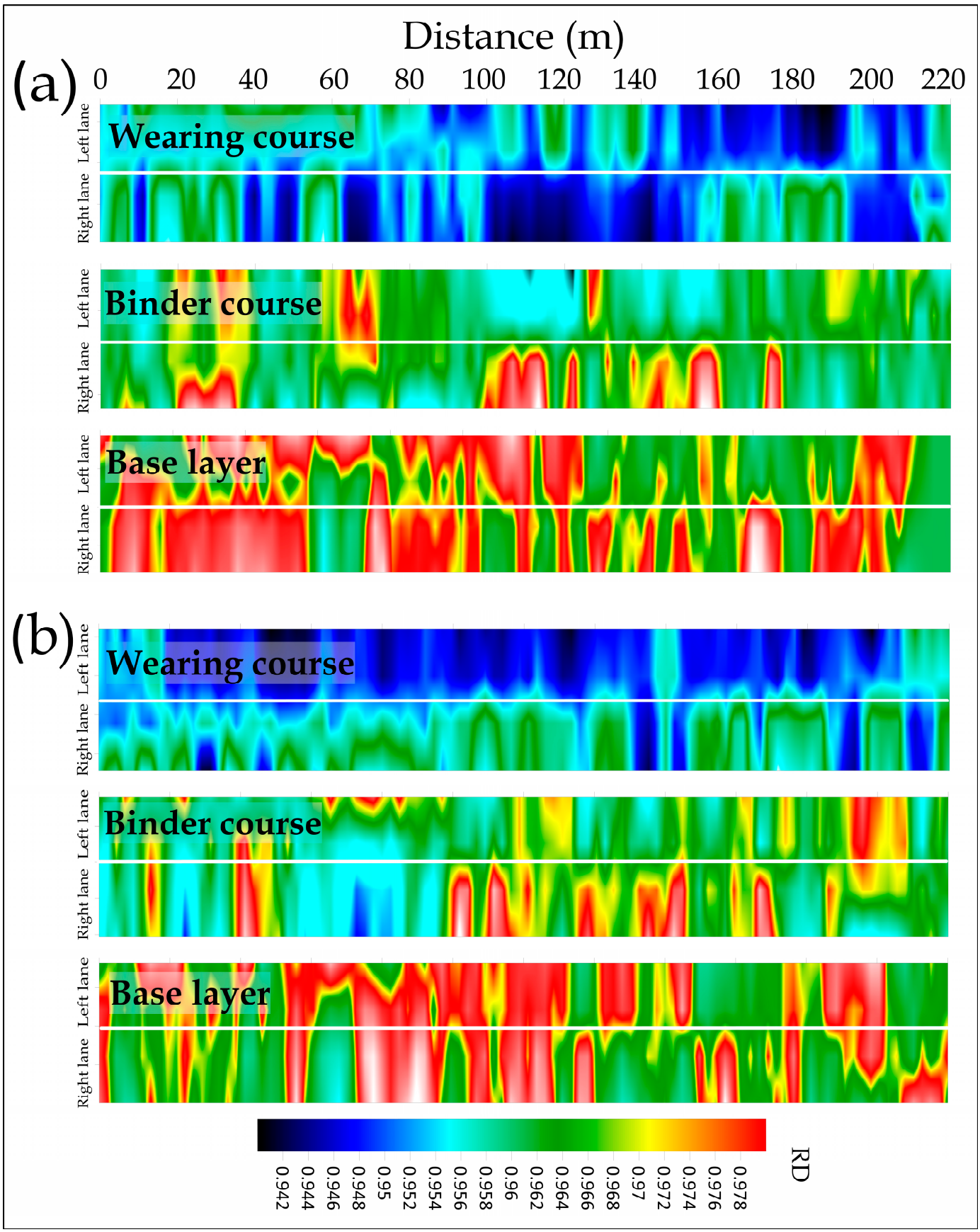

Figure 8. Horizontal variation of RD in terms of investigated layers: (**a**) Section I.; (**b**) Section II.

In addition to the layer-to-layer differences in the RD values, a significant within-layer inhomogeneity was also apparent in the investigated courses (Table 3). This is most striking when the right and left lanes, compacted separately, are compared to each other (Figure 7). The greatest difference in the compaction of separate lanes can be seen in terms of the wearing course; for example, at Section II., a 3.6% difference was identified between the average RD of the two lanes (Figure 8b). The density variation was significant along the same lane as well (Figure 8a,b), suggesting that the temperature of the asphalt mixture was changing during the construction process. Based on the results, additional roller passes should have been made during the construction of the wearing course, especially on the left lane at Section II. (Figure 8b). Although the general condition of the investigated section is good, the identified spatial differences in the compaction quality call for the continuous monitoring of the road structure.

7. Discussion

The assessment of pavement conditions is essential for efficient transportation infrastructure management. GPR technology provides different alternatives for assessing the dielectric properties of asphalt layers. However, these alternatives may yield significantly different results. Porubiaková and Komačka [6] found differences between the SR and TOF methods. The present study found that the SR method fits laboratory results better.

On the other hand, Wang et al. [5] found that a certain type of TOF method can provide equally good results. However, the common mid-point (CMP) approach allows for a real-time TOF-accurate estimation method, which involves more complex data acquisition and processing than simpler GPR survey techniques. It requires careful planning and execution and sophisticated processing software, which can increase the overall cost and time needed for the survey. Thus, SR was a simpler method that produced reliable measurements.

The study of the relationship between the ε and G_{mb} revealed a strong linear correlation regarding the wearing course, with a coefficient of determination (R^2) of 0.85. Similar findings were reported by several other authors, such as Chang et al. [32] and Popik et al. [33], using the same antenna frequency (2 GHz) and also by Xiong et al. [34]. However, they did not indicate the frequency of the applied antenna. These authors found R^2 values of 0.73, 0.71, and 0.81, respectively. However, the slope of their functions is different from those in the present study (Figure 9). The differences in slope can be attributed to several factors, including the aggregate composition and gradation, asphalt binder content, air voids, and compaction efficiency, as discussed by Chang et al. [32] in detail. Although the G_{mb} was measured using different methods (the density prediction model, non-nuclear density gauge, and nuclear density gauge), the obtained values were within a range of ± 0.05 g/cm^3, showing high consistency across the studies.

The data from the above studies are plotted in Figure 9. It is clear that even though the investigated HMA mixtures have different characteristics (Table 4), most of the data plot to the same region (Figure 9) and provide a means of determining a more general function between the ε and G_{mb} (Figure 10). We found that in the case of our study (Wearing course, Binder course, Base course) and the survey made by Xiong et al. [34] (AC 13, AC 20, AC 25), the data are located in the same range. However, in the present study, in the case of the sub-base layers, we found that the data fall outside the expected range of dielectric values (ε) due to the larger aggregate size (d_{max} = 30 mm). Additionally, the asphalt content plays a significant role in these deviations, as a higher asphalt content generally results in lower dielectric values due to the reduced volumetric proportions of mineral filler and aggregate.

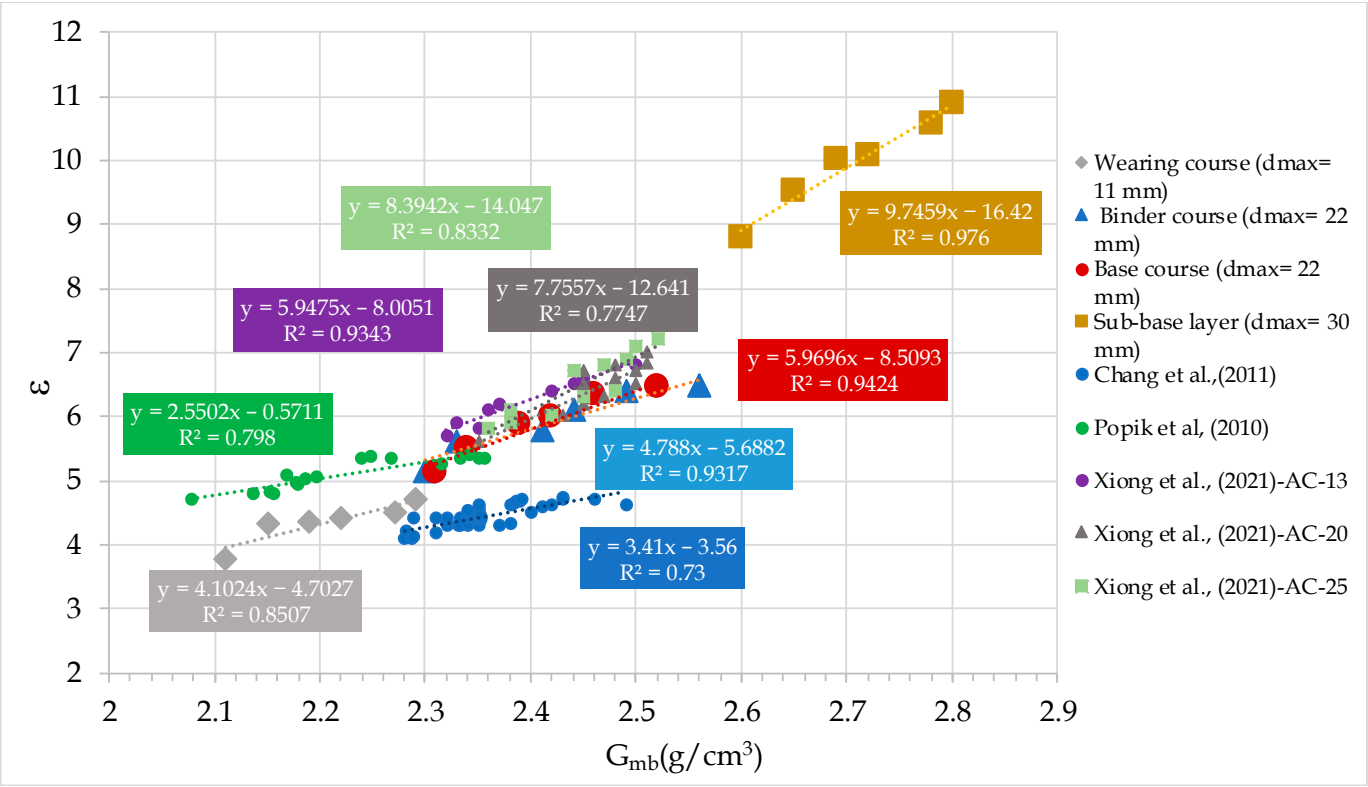

Figure 9. Comparison of relationship between ε and G_{mb} resulting from this study and other authors' studies [32–34].

Table 4. Mean, minimum, and maximum values and range and standard deviation of RD for investigated asphalt layers.

	Course Type	Mean RD	Min RD	Max RD	Range RD	SD
Section I.	Wearing course	0.949	0.944	0.956	0.012	0.033
	Binder course	0.964	0.960	0.971	0.011	0.022
	Base course	0.976	0.972	0.978	0.006	0.041
Section II.	Wearing course	0.944	0.942	0.954	0.012	0.037
	Binder course	0.963	0.962	0.974	0.012	0.029
	Base course	0.974	0.971	0.977	0.006	0.043

The impact of the asphalt binder content on dielectric values is particularly important in interpreting the results shown in Figure 8. The asphalt content influences the density and compaction of asphalt mixtures, thereby affecting the dielectric response. As seen in other studies [32,33], an increase in the asphalt binder content tends to decrease the overall dielectric constant due to the lower permittivity of the binder compared to the mineral aggregate. This relationship must be considered when comparing different datasets and developing generalized functions for dielectric estimation. Therefore, the variations in asphalt binder content should be explicitly analyzed alongside other influencing factors such as air voids, compaction efficiency, and aggregate gradation.

Finally, for asphalt pavements with aggregate sizes ranging from 11 mm to 25 mm, composed of limestone–dolomite, and within the same percentage of asphalt binder content as detailed in (Table 5), we propose a generalized function between the ε and G_{mb} for these specific conditions (Figure 10). The influence of the asphalt content on these correlations further highlights the necessity of considering binder properties in future analyses.

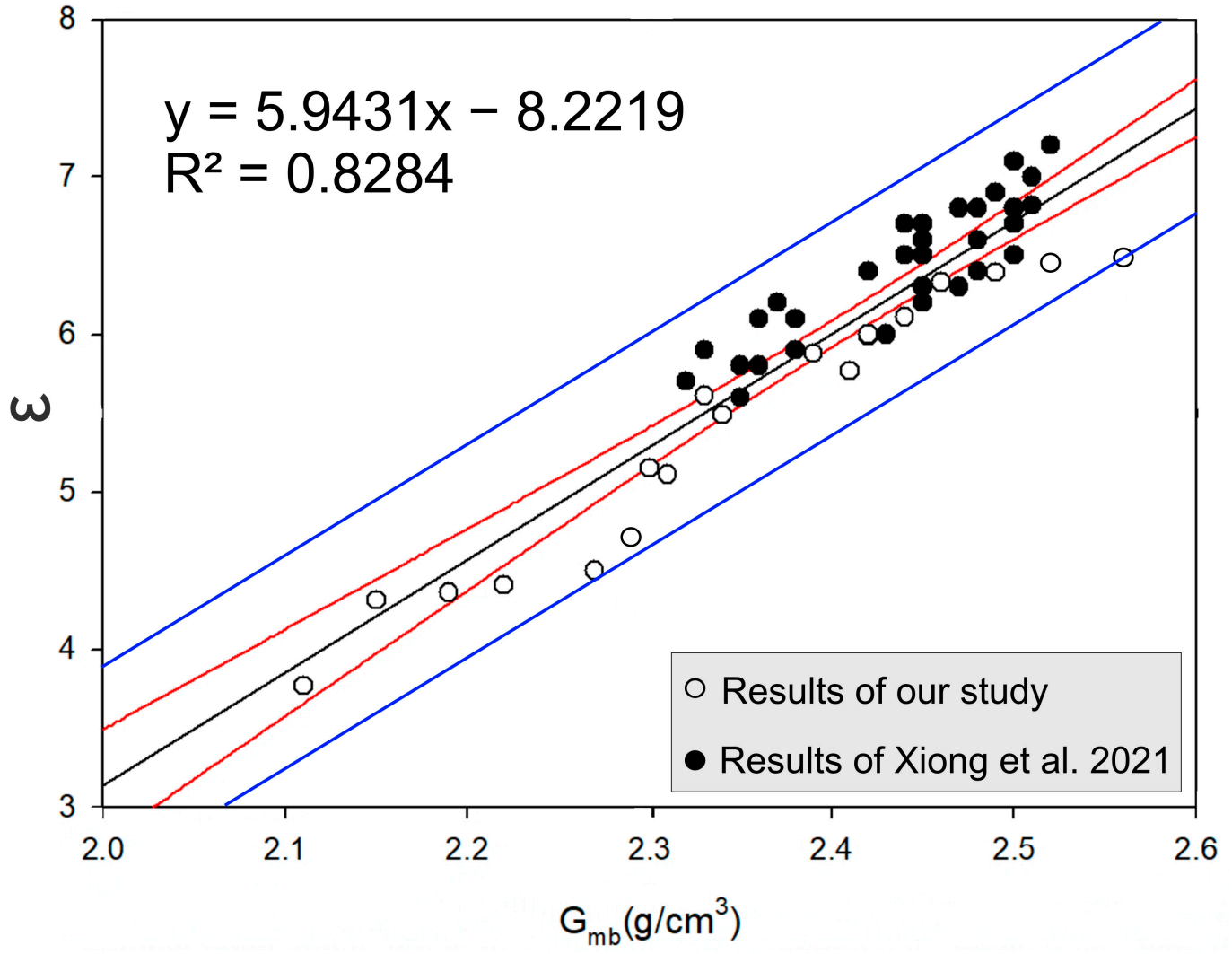

Figure 10. Plot of function between ε and G_{mb} derived from our study and Xiong et al. [34].

Table 5. Mineral composition, aggregate size, asphalt binder, mean ε, G_{mb}, and other information regarding studies plotted on Figure 9.

	This Study	**Popik et al. [33]**	**Xiong et al. [34]**	**Chang et al. [32]**
Mineral composition	Dolomitic limestone	Granite	Limestone	Sandstone
Aggregate size	AC 11, AC 22	AC 13–19 mm	AC 13, AC 20, AC 25	AC 20
Asphalt Binder	4.1%	5.1%	4.5%, 4.1%, 3.8%	4%, 5%, 6%
Mean ε	2.36	2.23	2.44	2.35
G_{mb}	5.45	5.11	6.43	4.44
Other	Binder RD: 1.050 g/cm^3	35% Recycled Asphalt Pavement (RAP)	8% Air voids, 0.44% Moisture content	2–10% Air voids

Based on our study, reflection amplitudes become relatively constant after six compaction passes. This finding was reinforced by Leng et al. [22], indicating that the maximum mixture densities can be achieved when the number of compaction passes reaches six. Another study by Zhao et al. [35] revealed that the rolling resistance and energy utilization coefficient values were less than 0 when the numbers of roller passes were 7, 9, and 10, since the value of the compaction energy density was at a very low level when the number of roller passes exceeded 6.

Despite the observed variations, the RD of asphalt layers in the investigated road section ranged between 0.94 and 0.98, which is considered close to the optimum value. These results are consistent with those reported by Popik et al. [33], who found that over 80% of the surveyed area exhibited RD values between 0.90 and 0.95. Another study by Zhao et al. [35] found that the degree of compaction ranged between 0.93 and 0.99; when they used different rollers, they found that the compaction effect for the same number of roller passes was different. Beainy et al. [36] found that approximately 99% of three other sites were compacted between a density of 0.93 and 0.96 by using the intelligent asphalt compaction analyzer (IACA); they also found that less than 1% of the completed pavement was undercompacted.

Finally, Commuri et al. [37] found that the RD values ranged between 0.91 and 0.93 when using a nonnuclear density gauge. All of the above results reiterate that most of the construction was of high quality.

Our results showed that the ε and RD values of the binder course were higher than those of the wearing course. This suggests that, beyond the influence of D_{max} and other factors, the wearing course exerted pressure on the binder course. Loizos and Plati [3] also found that the dielectric properties of the wearing course can influence the estimated values of the binder course. This can be explained by several factors: The weight of the asphalt layers increases the compression in the underlying layers, raising their density and affecting the dielectric properties. Temperature differences between layers may also influence the ε, as shown by Kassem et al. [38], who found that lower compaction temperatures increased air voids in both the HMA and WMA. Additionally, material composition variations and possible chemical or physical interactions between layers could contribute to changes in dielectric properties.

8. Conclusions

In the comparative analysis of dielectric values derived from the PaveScan and horn antenna measurements, the dielectric values measured by the horn antenna were more closely aligned with the core data. This suggests that the horn antenna measurements are highly effective in estimating ε, demonstrating superior accuracy compared to the PaveScan measurements. Based on the laboratory findings, we concluded that the SR derived from the horn antenna method can be effectively utilized for reliable pavement investigations.

Asphalt density assessments can be spatially extended by calibrating the GPR dielectric data using nuclear gauge measurements, and atomic measurements can be substituted. This is especially true regarding larger projects, in which the same, or a similar, AC mix is used on longer road sections. We concluded that the ε depended on the density of the asphalt mixture—a higher density reduced air voids, leading to an increased dielectric constant. Additionally, we proposed a generalized function to describe the relationship between the ε and bulk G_{mb} under specified conditions, such as asphalt pavements with aggregate sizes ranging from 11 mm to 25 mm and composed of dolomite or limestone. Therefore, we concluded that the asphalt content influenced the dielectric constant, as the density of the Hot Mix Asphalt (HMA) was influenced by the components of air, mineral filler, aggregate, and asphalt binder. The compaction curve helps determine the required number of compaction passes to achieve the maximum asphalt mixture density, and the GPR measurement corresponding to the maximum density can be used as a reference to examine the density levels at other locations.

The presented RD maps demonstrated that the relative compactness of in situ asphalt materials is not uniform. Variations in density within the same layer suggest variations in the compaction efficiency during construction. Specifically, Section II.'s left lane exhibited a lower compaction quality, indicating that additional roller passes should have been

made during the construction of the wearing course. Although the general condition of the investigated section is good, the identified spatial differences in compaction quality, particularly in Section II., justify continuous monitoring of the road structure. This need for monitoring is further supported by the observed density variations beyond an acceptable threshold, which could impact the long-term performance. Incorporating literature on pavement-monitoring decision making could further strengthen this justification.

We concluded that a method for density assessment was developed using GPR by surveying asphalt at different degrees of compaction. This way, more accurate RD maps were generated to visualize the spatial homogeneity of the density. The survey findings highlight that it is possible to indirectly determine the G_{mb} of asphalts composed of dolomite and limestone aggregates using horn antenna GPR measurements calibrated with nuclear gauge data, as these methods demonstrated superior accuracy and reliability in estimating the ε and assessing the asphalt density. In addition, the RD maps generated in this study are important in predicting the long-term performance of the pavement, supporting maintenance strategies, and facilitating the detection of different defects.

Author Contributions: Conceptualization, E.A. and D.S.; Methodology, E.A. and Z.T.; Data Processing, E.A. and D.S.; Physical Properties Analysis, E.A. and D.S.; Validation, E.A. and Z.T.; Formal Analysis, E.A. and D.S.; Investigation, E.A., A.M.A., K.B., A.F., G.M. and V.B.-V.; Resources, E.A.; Writing, original draft, E.A.; writing, reviewing, and editing, all authors; visualization, E.A., D.S. and G.S.; supervision, G.S.; project administration, G.S. All authors have read and agreed to the published version of the manuscript.

Funding: The GPR measurements were conducted with support from Roden Ltd. under project 2018-1.1.2-KFI-2018-00029, funded by the National Research, Development and Innovation Fund, Hungary.

Institutional Review Board Statement: Not applicable.

Informed Consent Statement: Not applicable.

Data Availability Statement: The data presented in this study are available on request from the corresponding author. The data are not publicly available due to institutional policies.

Acknowledgments: We would like to acknowledge Boglárka Runa's and Olivér Balogh's contributions during the geophysical data acquisition.

Conflicts of Interest: There are no conflicts of interest to declare.

References

1. Daniels, D.J. (Ed.) *Ground Penetrating Radar*; IET: Stevenage, UK, 2004; Volume 1.
2. Al-Qadi, I.L.; Lahouar, S. Measuring layer thicknesses with GPR–Theory to practice. *Constr. Build. Mater.* **2005**, *19*, 763–772. [CrossRef]
3. Loizos, A.; Plati, C. Accuracy of Ground Penetrating Radar Horn-Antenna Technique for Sensing Pavement Subsurface. *IEEE Sens. J.* **2007**, *7*, 842–850. [CrossRef]
4. Loizos, A.; Plati, C. Accuracy of pavement thicknesses estimation using different ground penetrating radar analysis approaches. *NDT E Int.* **2007**, *40*, 147–157. [CrossRef]
5. Wang, S.; Leng, Z.; Sui, X.; Zhang, W.; Ma, T.; Zhu, Z. Real-Time Asphalt Pavement Layer Thickness Prediction Using Ground-Penetrating Radar Based on a Modified Extended Common Mid-Point (XCMP) Approach. *IEEE Trans. Intell. Transp. Syst.* **2024**, *25*, 6848–6860. [CrossRef]
6. Porubiaková, A.; Komačka, J. A Comparison of Dielectric Constants of Various Asphalts Calculated from Time Intervals and Amplitudes. *Procedia Eng.* **2015**, *111*, 660–665. [CrossRef]
7. Abdelsamei, E.; Sheishah, D.; Runa, B.; Balogh, O.; Tóth, C.; Primusz, P.; Trenka, S.; van Leeuwen, B.; Tobak, Z.; Páll, D.G.; et al. Application of Ground Penetrating Radar in the Assessment of Aged Roads: Focus On Complex Structures Under Different Weather Conditions. *Pure Appl. Geophys.* **2024**, *181*, 3633–3651. [CrossRef]
8. Abdelsamei, E.; Sheishah, D.; Aldeep, M.; Tóth, C.; Sipos, G. Defect Recognition: Applying Time-Lapse GPR Measurements and Numerical Approaches. *Eng* **2025**, *6*, 5. [CrossRef]

9. Sarabandi, K.; Li, E.; Nashashibi, A. Modeling and measurements of scattering from road surfaces at millimeter-wave frequencies. *IEEE Trans. Antennas Propag.* **1997**, *45*, 1679–1688. [CrossRef]
10. Al-Qadi, I.L.; Lahouar, S.; Loulizi, A. In situ measurements of hot-mix asphalt dielectric properties. *NDT E Int.* **2001**, *34*, 427–434. [CrossRef]
11. Ghosh, S.; Kundu, S. Fluvial anomaly as indicator of tectonically active landscapes: A study in the Darjeeling Sikkim Himalaya, India. *DYSONA-Appl. Sci.* **2025**, *6*, 70–85. [CrossRef]
12. Primusz, P.; Abdelsamei, E.; Ali, A.M.; Sipos, G.; Fi, I.; Herceg, A.; Tóth, C. Assessment of In Situ Compactness and Air Void Content of New Asphalt Layers Using Ground-Penetrating Radar Measurements. *Appl. Sci.* **2024**, *14*, 614. [CrossRef]
13. Keller, G.V. Electrical properties of rocks and minerals. In *Handbook of Physical Properties of Rocks (1982)*; CRC Press: Boca Raton, FL, USA, 2017; pp. 217–294.
14. Šernas, O.; Vorobjovas, V.; Šneideraitienė, L.; Vaitkus, A. Evaluation of Asphalt Mix with Dolomite Aggregates for Wearing Layer. *Transp. Res. Procedia* **2016**, *14*, 732–737. [CrossRef]
15. ElShafie, A.; Heggy, E. Dielectric and hardness measurements of planetary analog rocks in support of in-situ sub-surface sampling. *Planet. Space Sci.* **2013**, *86*, 150–154. [CrossRef]
16. Hartlieb, P.; Toifl, M.; Kuchar, F.; Meisels, R.; Antretter, T. Thermo-physical properties of selected hard rocks and their relation to microwave-assisted comminution. *Miner. Eng.* **2016**, *91*, 34–41. [CrossRef]
17. Roberts, F.L.; Kandhal, P.S.; Brown, E.R.; Lee, D.Y.; Kennedy, T.W. *Hot Mix Asphalt Materials, Mixture Design and Construction*; National Asphalt Pavement Association: Greenbelt, MD, USA, 1996.
18. Brown, E. Density of asphalt concrete-how much is needed? In Proceedings of the 69th Annual Meeting of the Transportation Research Board, Washington, DC, USA, 9–11 January 1990. [CrossRef]
19. Saarenketo, T. Using Ground-Penetrating Radar and Dielectric Probe Measurements in Pavement Density Quality Control. *Transp. Res. Rec. J. Transp. Res. Board* **1997**, *1575*, 34–41. [CrossRef]
20. Saarenketo, T.; Roimela, P. Ground penetrating radar technique in asphalt pavement density quality control. In Proceedings of the Seventh International Conference on Ground Penetrating Radar, Lawrence, KS, USA, 27–30 May 1998; Volume 2, pp. 461–466.
21. Willoughby, K.; Mahoney, J. *An Assessment of Wsdot's Hot-Mix Asphalt Quality Control and Assurance Requirements*; Resreport WA-RD 517.2; Washington State Department of Transportation: Olympia, WA, USA, 2007.
22. Leng, Z.; Al-Qadi, I.L.; Shangguan, P.; Son, S. Field Application of Ground-Penetrating Radar for Measurement of Asphalt Mixture Density: Case Study of Illinois Route 72 Overlay. *Transp. Res. Rec. J. Transp. Res. Board* **2012**, *2304*, 133–141. [CrossRef]
23. Shangguan, P.; Al-Qadi, I.; Coenen, A.; Zhao, S. Algorithm development for the application of ground-penetrating radar on asphalt pavement compaction monitoring. *Int. J. Pavement Eng.* **2016**, *17*, 189–200. [CrossRef]
24. Maser, K.R. Condition Assessment of Transportation Infrastructure Using Ground-Penetrating Radar. *J. Infrastruct. Syst.* **1996**, *2*, 94–101. [CrossRef]
25. Saarenketo, T.; Scullion, T. Road evaluation with ground penetrating radar. *J. Appl. Geophys.* **2000**, *43*, 119–138. [CrossRef]
26. Romero, P.; Kuhnow, F. Evaluation of New Nonnuclear Pavement Density Gauges with Data from Field Projects. *Transp. Res. Rec. J. Transp. Res. Board* **2002**, *1813*, 47–54. [CrossRef]
27. Al-Qadi, I.L.; Leng, Z.; Lahouar, S.; Baek, J. In-Place Hot-Mix Asphalt Density Estimation Using Ground-Penetrating Radar. *Transp. Res. Rec. J. Transp. Res. Board* **2010**, *2152*, 19–27. [CrossRef]
28. Geophysical Survey Systems Incorporation (GSSI). *RADAN 7 Manual (2023)*; Geophysical Survey Systems, Inc.: Nashua, NH, USA, 2017. Available online: https://www.geophysical.com/wp-content/uploads/2017/10/GSSI-RADAN-7-Manual.pdf (accessed on 20 September 2023).
29. InstroTek, I. MC-3 EliteTM | InstroTek, Inc. n.d. Available online: https://www.instrotek.com/products/mc-3-elite (accessed on 10 April 2022).
30. Pavement Interactive. Nuclear Density Gauge—Pavement Interactive. 2002. Available online: https://pavementinteractive.org/reference-desk/construction/compaction/nuclear-density-gauge/ (accessed on 20 October 2023).
31. Li, J.; Walubita, L.F.; Simate, G.S.; Alvarez, A.E.; Liu, W. Use of ground-penetrating radar for construction monitoring and evaluation of perpetual pavements. *Nat. Hazards* **2013**, *75*, 141–161. [CrossRef]
32. Chang, C.-M.; Chen, J.-S.; Wu, T.-B. Dielectric Modeling of Asphalt Mixtures and Relationship with Density. *J. Transp. Eng.* **2011**, *137*, 104–111. [CrossRef]
33. Popik, M.; Maser, K.; Holzschuher, C. Using high-speed ground penetrating radar for evaluation of asphalt density measurements. In Proceedings of the Annual Conference & Exhibition of the Transportation Association of Canada, Halifax, NS, Canada, 26–29 September 2010; pp. 26–29.
34. Xiong, X.; Xiao, S.; Tan, Y.; Zhang, X.; Zhang, D.; Han, M.; Wang, W. Estimation of density and moisture content in asphalt mixture based on dielectric property. *Constr. Build. Mater.* **2021**, *298*, 123518. [CrossRef]
35. Zhao, Y.; Xie, S.; Gao, Y.; Zhang, Y.; Zhang, K. Prediction of the number of roller passes and degree of compaction of asphalt layer based on compaction energy. *Constr. Build. Mater.* **2021**, *277*, 122274. [CrossRef]

36. Beainy, F.; Commuri, S.; Zaman, M. Quality Assurance of Hot Mix Asphalt Pavements Using the Intelligent Asphalt Compaction Analyzer. *J. Constr. Eng. Manag.* **2012**, *138*, 178–187. [CrossRef]
37. Commuri, S.; Mai, A.T.; Zaman, M. Neural Network–Based Intelligent Compaction Analyzer for Estimating Compaction Quality of Hot Asphalt Mixes. *J. Constr. Eng. Manag.* **2011**, *137*, 634–644. [CrossRef]
38. Kassem, E.; Scullion, T.; Masad, E.; Chowdhury, A. Comprehensive Evaluation of Compaction of Asphalt Pavements and a Practical Approach for Density Predictions. *Transp. Res. Rec. J. Transp. Res. Board* **2012**, *2268*, 98–107. [CrossRef]